Ideal charge-density-wave order in the high-field state of superconducting YBCO

H. Jang[a,1], W.-S. Lee[b,1], H. Nojiri[c], S. Matsuzawa[c], H. Yasumura[c], L. Nie[d], A. V. Maharaj[d], S. Gerber[e], Y.-J. Liu[a], A. Mehta[a], D. A. Bonn[f,g], R. Liang[f,g], W. N. Hardy[f,g], C. A. Burns[a,h], Z. Islam[i], S. Song[j], J. Hastings[j], T. P. Devereaux[b], Z.-X. Shen[b,d], S. A. Kivelson[d,2], C.-C. Kao[k], D. Zhu[j,2], and J.-S. Lee[a,1,2]

[a]Stanford Synchrotron Radiation Lightsource, SLAC National Accelerator Laboratory, Menlo Park, CA 94025; [b]Stanford Institute for Materials and Energy Science, SLAC National Accelerator Laboratory and Stanford University, Menlo Park, CA 94025; [c]Institute for Materials Research, Tohoku University, Katahira 2-1-1, Sendai 980-8577, Japan; [d]Geballe Laboratory for Advanced Materials, Departments of Physics and Applied Physics, Stanford University, Stanford, CA 94305; [e]SwissFEL, Paul Scherrer Institut, 5232 Villigen PSI, Switzerland; [f]Department of Physics & Astronomy, University of British Columbia, Vancouver, BC, Canada V6T 1Z1; [g]Canadian Institute for Advanced Research, Toronto, ON, Canada M5G 1Z8; [h]Department of Physics, Western Michigan University, Kalamazoo, MI 49008; [i]The Advanced Photon Source, Argonne National Laboratory, Argonne, IL 60439; [j]Linac Coherent Light Source, SLAC National Accelerator Laboratory, Menlo Park, CA 94025; and [k]SLAC National Accelerator Laboratory, Menlo Park, CA 94025

Contributed by Steven A. Kivelson, November 4, 2016 (sent for review August 4, 2016; reviewed by Peter Abbamonte and Patrick A. Lee)

The existence of charge-density-wave (CDW) correlations in cuprate superconductors has now been established. However, the nature of the CDW ground state has remained uncertain because disorder and the presence of superconductivity typically limit the CDW correlation lengths to only a dozen unit cells or less. Here we explore the field-induced 3D CDW correlations in extremely pure detwinned crystals of $YBa_2Cu_3O_x$ (YBCO) ortho-II and ortho-VIII at magnetic fields in excess of the resistive upper critical field (H_{c2}) where superconductivity is heavily suppressed. We observe that the 3D CDW is unidirectional and possesses a long in-plane correlation length as well as significant correlations between neighboring CuO_2 planes. It is significant that we observe only a single sharply defined transition at a critical field proportional to H_{c2}, given that the field range used in this investigation overlaps with other high-field experiments including quantum oscillation measurements. The correlation volume is at least two to three orders of magnitude larger than that of the zero-field CDW. This is by far the largest CDW correlation volume observed in any cuprate crystal and so is presumably representative of the high-field ground state of an "ideal" disorder-free cuprate.

high-temperature superconductors | charge-density-wave order | high magnetic field X-ray scattering | vestigial nematic order | competing order

Charge-density-wave (CDW) order has been found to exist universally in the hole-doped superconducting cuprates (1–18), and the common characteristics at zero magnetic field include bidirectionality, quasi-2D and short-ranged correlations (7–17). More specifically, the CDW diffraction patterns are found in both directions of Cu–O bonds in the CuO_2 plane (Fig. 1*A*), and the CDW correlation lengths parallel and perpendicular to the planes (i.e., along the a- or b-axes and the c axis) are less than ~ 20 and ~ 1 lattice constants, respectively (7–16), corresponding to a correlation volume of order 10^2 unit cells (UCs). Thus, the properties of the quasi-2D CDW are likely strongly affected by disorder and only indirectly represent the true nature of the underlying CDW correlations. Indeed, X-ray scattering shows that the onset of the quasi-2D order is gradual without a sharp transition (7–17), consistent with the influence of quenched disorder on an incommensurate CDW (19–21). Furthermore, whereas Y-based and La-based cuprates exhibit a clear competition between CDW and superconductivity (7, 8, 12–15), such competition is not apparent in the families of Bi-based and Hg-based cuprate compounds (9–11)—a discrepancy that probably reflects different degrees of quenched disorder among cuprate families.

Recently, a CDW with significantly longer correlation lengths was observed in superconducting YBCO (Fig. 1*B*) via X-ray scattering at high magnetic fields (13, 14). This reveals the character (i.e., 3D) of the high-field charge ordering previously inferred by other measurements (3–6). At a magnetic field of ~ 30 T, its in- and out-of-plane correlation lengths are of the order of 100 and 10 lattice constants, respectively (13, 14), which are significantly larger than those of the zero-field 2D CDW. Thus, it arguably represents the CDW ground state of an "ideal" disorder-free cuprate superconductor. However, to date, although this 3D CDW has been reported at doping levels of $p\sim 0.12$ and ~ 0.11 (13, 14), limited high-field data near H_{c2} are only available at $p\sim 0.12$ (13). To establish the 3D CDW phenomenology, it is important to track its doping and magnetic field dependences up to H_{c2} and to elucidate its puzzling relationship with the quasi-2D CDW that coexists with the 3D one even at high field (Fig. 1*B*) (13, 14).

Results

To address these issues, we first investigate detwinned YBCO ortho-II ($x = 6.51$) using X-ray scattering at an X-ray free

Significance

Compelling evidence of various forms of nonsuperconducting electronic order in the cuprate high-temperature superconductors has fundamentally altered our understanding of the essential physics of these materials. However, it has been difficult to establish the nature of the quantum (zero-temperature) phases that compete and/or coexist with superconductivity. By studying high-quality crystals of YBCO using an X-ray laser and pulsed magnetic fields, we have established that the field induced charge-density-wave (CDW) order that arises when superconductivity is suppressed at low temperatures is incommensurate, unidirectional, and 3D-ordered. While disorder ultimately precludes true CDW long-range order, there does appear to be a sharply defined crossover field, which we associate with a transition to a nematic state with long-range orientational order.

Author contributions: W.-S.L., H.N., C.-C.K., D.Z., and J.-S.L. designed research; H.J., W.-S.L., H.N., S.M., H.Y., L.N., A.V.M., S.G., Y.-J.L., D.A.B., J.H., S.A.K., D.Z., and J.-S.L. performed research; H.J., W.-S.L., L.N., A.V.M., Y.-J.L., A.M., D.A.B., R.L., W.N.H., C.A.B., Z.I., S.S., J.H., T.P.D., Z.-X.S., S.A.K., C.-C.K., and J.-S.L. analyzed data; and H.J., W.-S.L., H.N., L.N., A.V.M., J.H., T.P.D., Z.-X.S., S.A.K., C.-C.K., D.Z., and J.-S.L. wrote the paper.

Reviewers: P.A., University of Illinois; and P.A.L., Massachusetts Institute of Technology.

The authors declare no conflict of interest.

Freely available online through the PNAS open access option.

[1]H.J., W.-S.L., and J.-S.L. contributed equally to this work.

[2]To whom correspondence may be addressed. Email: kivelson@stanford.edu, dlzhu@slac.stanford.edu, or jslee@slac.stanford.edu.

This article contains supporting information online at www.pnas.org/lookup/suppl/doi:10.1073/pnas.1612849113/-/DCSupplemental.

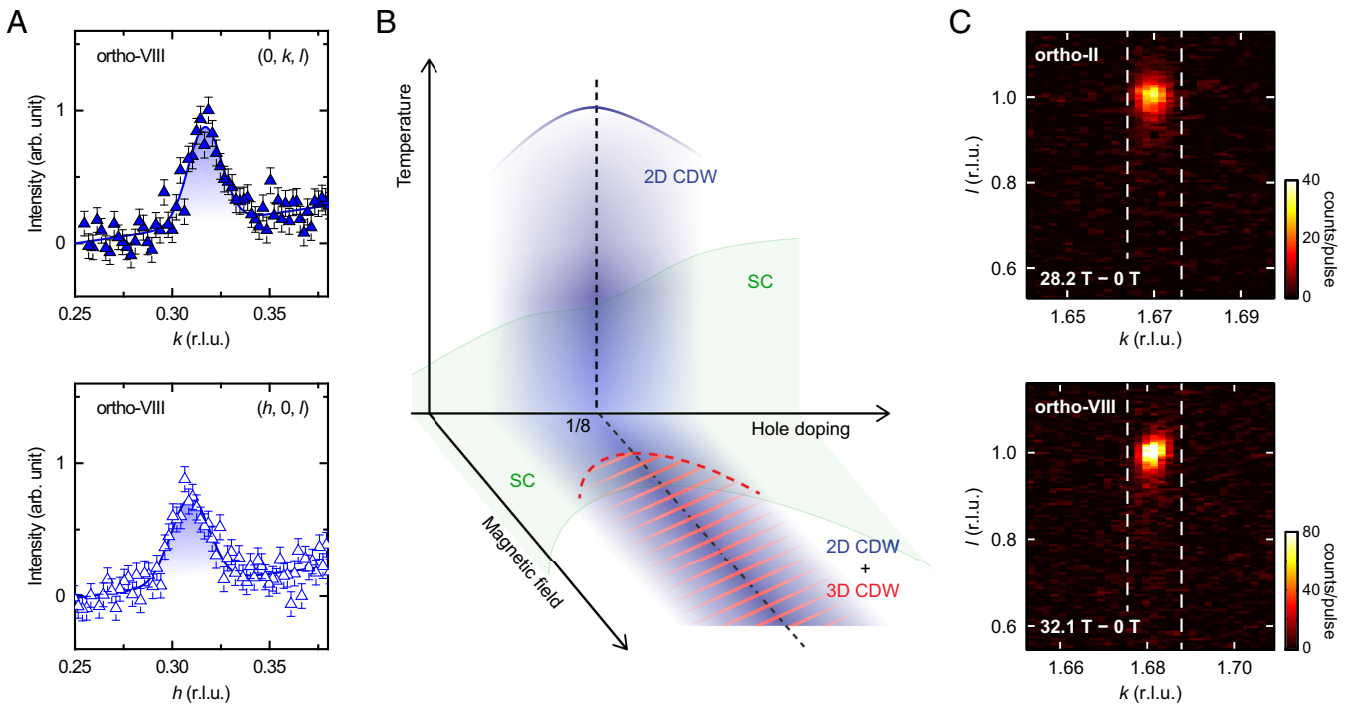

Fig. 1. CDW orders in $YBa_2Cu_3O_x$ (YBCO). (*A*) Zero-field quasi-2D CDW diffraction peak profiles (*Upper* and *Lower*) of ortho-VIII in the *k*- and *h*-directions, respectively, measured by resonant soft X-ray scattering at Cu L_3-edge and $T = 67$ K (*Materials and Methods*). It is bidirectional (i.e., the diffraction peaks are found in both Cu–O bond directions in the CuO_2 plane). (*B*) A schematic sketch of the temperature-doping-magnetic field phase diagram of YBCO near a hole concentration $p = 1/8$. The quasi-2D CDW (blue shaded area) evolves from high temperature and exists at both zero and finite magnetic fields. The 3D CDW (red-colored, hatched area) emerges only in high magnetic fields and at low temperatures but coexists with the 2D one (*SI Appendix*, Fig. S2*B*). (*C*) Maps of the difference between the diffraction intensities at high field and zero field in ortho-II (*Upper*) and ortho-VIII (*Lower*) (*SI Appendix*, Fig. S2*A*). The bright spots are the 3D CDW diffraction patterns located at $\mathbf{Q} \sim (0, 2 - q, 1)$, where q is ~ 0.33 in reciprocal lattice units (r.l.u.) and ~ 0.32 r.l.u. for ortho-II and ortho-VIII, respectively. The white dashed lines indicate the windows used to extract the projected peak profile shown in Figs. 2 and 4.

electron laser (FEL) combined with a pulsed magnet (13) (*Materials and Methods*). With $\mu_0 H = 28.2$ T, we clearly observe a field-induced CDW at $\mathbf{Q} = (0, 2 - q, 1)$ with an incommensurate $q \sim 0.33$ r.l.u (Fig. 1*C*). Similar to the case of YBCO ortho-VIII (13), the field-induced 3D CDW exhibits the same q-value as that of the zero-field quasi-2D CDW but with an integer rather than a half-integer l-value (8, 15). Note that the quasi-2D CDW still exists at this field (*SI Appendix*, Fig. S2*B*), confirming its coexistence with the 3D CDW.

The emergence of the 3D CDW order in YBCO ortho-II as a function of magnetic field is shown in Fig. 2*A*. As shown in the peak intensity at $l \sim 1$ (Fig. 2*B*), the 3D CDW appears at $\mu_0 H_{3D} \sim 18$ T. Further increase of the magnetic field not only increases the diffraction peak intensity but also narrows the peak width along both the l- and k-directions (Fig. 2*C*). At 28.2 T and 10 K, the ortho-II correlation lengths in the k- and l-directions are more than 230 Å (which is limited by our instrument resolution) and 55 Å, respectively. Furthermore, the 3D CDW shows strong temperature dependence (Fig. 2*D*). At $\mu_0 H = 26.0$ T, the projected peak intensity (Fig. 2*E*) and correlation length (Fig. 2*F*) demonstrated the appearance of the 3D CDW at $T_{3D} \sim 45$ K, which is considerably lower than the onset temperature of the quasi-2D CDW ($\sim$120 K), but just slightly lower than T_c (57 K at 0 T). Note that the onset field and temperature agree well with the thermodynamic phase boundary deduced from sound velocity measurements (5). Altogether, the H- and T-dependences demonstrate that 3D CDW emergence is triggered by the magnetic field suppression of superconducting correlations.

The field dependence of the 3D CDW in YBCO ortho-II is similar to that previously observed in ortho-VIII (13). As shown in Fig. 3*A*, if plotted as a function of shifted magnetic field (i.e., $\mu_0 H - \mu_0 H_{3D}$), the growth rate of the normalized 3D CDW intensity is remarkably similar in the two crystals, despite the different doping concentrations. Furthermore, both crystals exhibit a similar quantitative evolution of the 3D CDW correlation volume, which reaches $\sim 10^5$ UCs at $H \sim H_{c2}$ (Fig. 3*B*)—more than two orders larger than that of the quasi-2D order. Interestingly, the ratio H_{3D}/H_{c2} is $\sim$0.6 for both crystals, suggesting that H_{3D} closely tracks H_{c2}, a key characteristic of the superconducting state. These findings further demonstrate the intimate relation between the 3D CDW and superconductivity, as well as supporting the attribution of the 3D CDW order as representative of the "disorder-free" situation.

Finally, we investigate signatures of the 3D CDW at an ordering wavevector in the h-direction at $\sim H_{c2}$ (22). Although the zero-field 2D CDW is bidirectional (e.g., Fig. 1*A*) (16, 17), it was discovered in ref. 14 that the 3D CDW in ortho-VIII is unidirectional (i.e., there is no detectable 3D CDW in the h-direction). Since those experiments only went up to 16.9 T, which is just $\sim$2 T above H_{3D}, it was still unclear whether the unidirectionality is an essential feature of the 3D CDW, as the possibility of an onset of 3D CDW in the h-direction at a slightly higher critical field could not be discarded. In our measurement up to 25 T no sign of the CDW pattern in ortho-VIII is seen near $l = 1$, as displayed in Fig. 4*A*, *Upper*. This is also evident in the featureless projected intensity along the l-direction (Fig. 4*A*, *Lower*) at $\mathbf{Q} = (1.68, 0, 1)$, in stark contrast to that at $\mathbf{Q} = (0, 1.68, 1)$. Thus, we establish that the order in ortho-VIII remains unidirectional and there is no further transition up to 25 T, in excess of H_{c2} and more than 50% above H_{3D}. Furthermore, we have performed the same measurement on ortho-II (Fig. 4*B*). Similarly, we find no

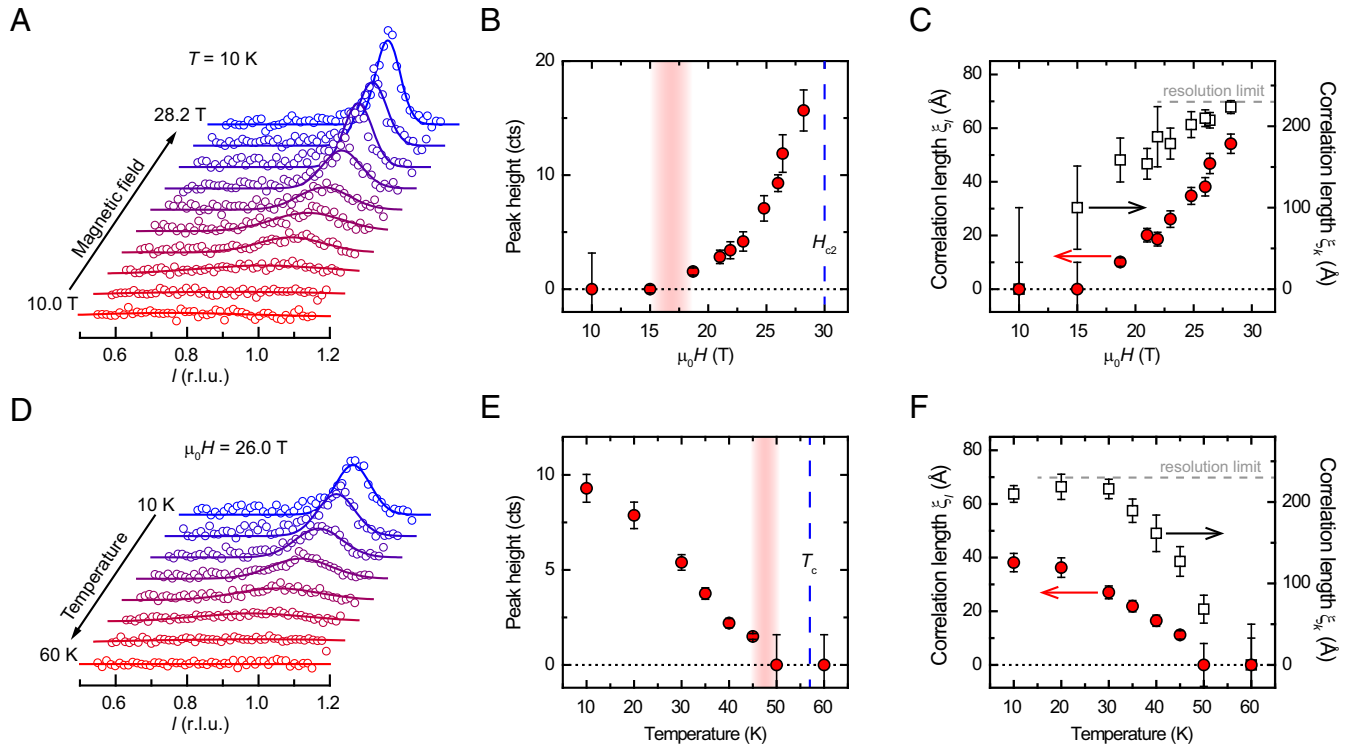

Fig. 2. Field and temperature dependences of the 3D CDW in ortho-II. (*A* and *D*) Projected peak profile along (0, 1.67, *l*) as a function of magnetic field at $T = 10$ K (*A*) and as a function of temperature at $\mu_0 H = 26.0$ (*D*). The data points are obtained by integrating the field-induced signal over the range of *k* indicated by the dashed line in Fig. 1*C*. Solid lines are Gaussian fits to the data. Note that the *kl* difference maps in the corresponding *H* and *T* are shown in *SI Appendix*, Fig. S3. (*B* and *C*) Fitted 3D CDW peak heights (*B*) and correlation lengths (*C*) in the *l*- and *k*-directions as a function of magnetic field. (*E* and *F*) Fitted 3D CDW peak heights (*E*) and correlation lengths (*F*) in the *l*- and *k*-directions as a function of temperature. The red shaded area denotes the onset region of the 3D CDW. Note that the *k*-correlation lengths at large *H* and low *T* are resolution-limited (~230 Å, indicated by the gray dashed lines in *E* and *F*); thus, they represent lower bounds of the actual values. The displayed ξ_k have been not corrected for an instrument resolution. All dotted lines indicate zero. The error bars denote 1 SD as obtained from the peak fitting.

3D CDW up to 30 T, which overlaps the range of field where quantum oscillations are observed (23). Altogether, we establish that 3D CDW in YBCO is robustly unidirectional; the 3D CDW is "stripe-like" with an ordering vector parallel to the Cu–O chain direction.

Discussion

We now discuss the puzzling relation between the unidirectional 3D CDW and the bidirectional 2D CDW. The drastic differences in the qualitative behaviors, including their directionality (13–16), dimensionality (8, 13–15), and their H- and T-dependences (8, 13–16), suggest that the unidirectional 3D CDW is a different entity from the quasi-2D CDW (7, 8, 15, 16). However, the diffraction signals from the 2D and 3D CDWs coexist (13, 14). It seems to us that the most promising way to reconcile these observations is to assume that there are distinct domains with the two types of CDW. However, the fact that the in-plane wavevectors of the two CDWs are identical suggests that they share the same local correlations inherent in the electronic structure of YBCO. Because the 3D CDW is unidirectional, we argue that the inherent CDW correlations correspond to unidirectional charge stripes.

On theoretical ground (19), an incommensurate CDW phase exists as a sharply defined phase of matter (i.e., with true long-range order) only in the ideal limit of vanishing disorder. However, as shown in Fig. 5, for a unidirectional CDW in a tetragonal system, a sharply defined nematic phase, a form of "vestigial" CDW order (19) that spontaneously breaks the point-group symmetry, exists so long as the disorder strength, σ, is less than a finite critical value, σ_c. The phase transition at $\sigma = \sigma_c$ is rounded in an orthorhombic system, but so long as the symmetry breaking field is weak there remains a sharp cross-over from an approximately bidirectional phase (i.e., isotropic) for $\sigma > \sigma_c$ to a strongly unidirectional phase for $\sigma < \sigma_c$. The bidirectional phase can still be locally stripe-like (17), but with the orientation of the stripes determined by the local disorder potential rather than by the orthorhombicity. Indeed, a strong tendency to nematic order (oriented by the weak orthorhombicity of YBCO) has been inferred from various experiments (24–26). In *SI Appendix* we illustrate these points using an effective field theory and also address the cross over from 2D to 3D correlations at σ_c.

This leads us to interpret our results as suggestive of a universal tendency toward unidirectional incommensurate CDW order in YBCO and a somewhat nonuniform distribution of the disorder strengths. The important theoretical point is that the existence of a critical disorder σ_c implies that small variations in the values of a single parameter (i.e., disorder strength, σ) can produce the multiple qualitative differences between the 2D and 3D signals, consistent with the assumption that the local CDW order is the same everywhere. This is also illustrated in Fig. 5. Upon the application of field, the isotropic 2D CDW in the less-disordered region (σ_{Less}) transforms into the nematic 3D CDW phase, whereas that in the more-disordered region (σ_{More}) still remains in the isotropic phase. This conjecture is consistent with the field-induced nematicity of the CDW near vortex cores hinted in a recent scanning tunneling microscope study on the double-layer Bi-based cuprate (27), in which the influence of disorder is stronger than in YBCO.

PHYSICS

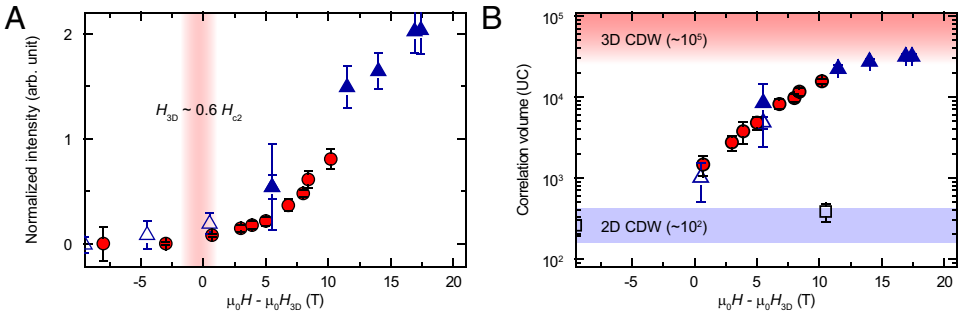

Fig. 3. Comparison of 3D CDWs in the ortho-II and ortho-VIII. (*A*) Fitted 3D CDW peak height of ortho-II (circles) and ortho-VIII (triangles) as a function of $\mu_0H-\mu_0H_{3D}$. Here, H_{3D} is 14.5 T and 18 T for the ortho-VIII (13, 14) and ortho-II crystals, respectively. The peak heights are normalized to 1 at H_{c2}. The values of resistive H_{c2} are adapted from ref. 22: 24 T and 30 T for our ortho-VIII and ortho-II crystals, respectively. The red shaded area denotes the onset region of the 3D CDW. Data of open triangles were taken from ref. 13. (*B*) Estimated 3D CDW correlation volumes of ortho-II (circles) and ortho-VIII (open/closed triangles) as a function of $\mu_0H-\mu_0H_{3D}$. To estimate the correlation volume, we have assumed that the correlation length along the *h*-direction is the same as along the *k*-direction for the 3D CDW at (0, 2-*q*, 1). Note that the in-plane correlation length used in this estimate is resolution-limited, so the estimated volume is a lower bound. The gray shaded area denotes the 2D CDW volume in ortho-VIII; data marked by the open squares (i.e., 2D CDW volumes) were taken from ref. 13. Error bars correspond to 1 SD.

One might expect that the integrated intensity in the 2D CDW peak would decrease above H_{3D} as the CDW changes its character in a portion of the sample. However, at the same time the CDW amplitude is also reinforced by the suppression of the superconductivity (*SI Appendix*). Because the CDW scattering intensity is determined by two compensating factors, the CDW amplitude and its volume fraction, the integrated intensity of the 2D CDW does not necessarily decrease (13, 14).

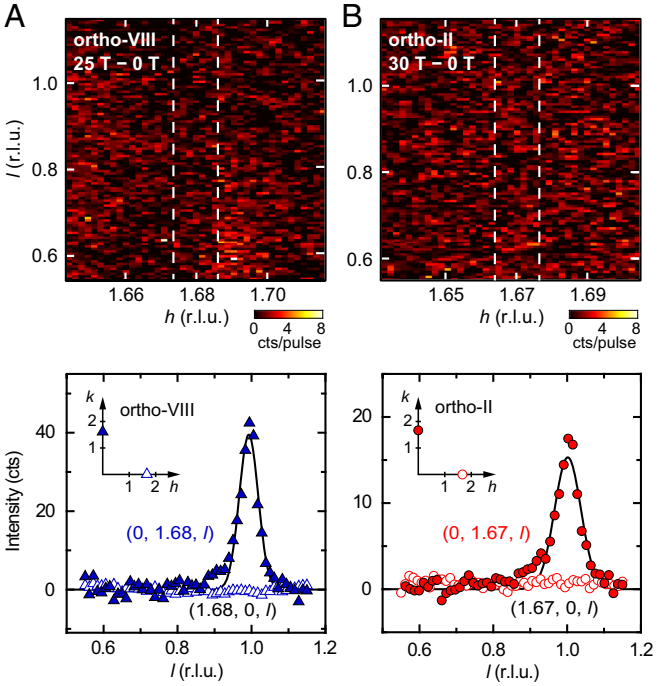

Fig. 4. Unidirectional character of the 3D CDW. Zero-field-background subtracted diffraction intensity maps of ortho-VIII (*A*) and ortho-II (*B*) in high magnetic fields and in the *hl*-reciprocal plane (*Upper*). (*Lower*) The projected intensities along (1.68, 0, *l*) (blue open triangles) and (0, 1.68, *l*) (blue closed triangles) in ortho-VIII and (1.67, 0, *l*) (red open circles) and (0, 1.67, *l*) (red closed circles) in ortho-II. The projected intensity is obtained by integrating the signal within the window indicated by the dashed lines in *A* and *B*, *Upper* and Fig. 1*C*. Solid lines are Gaussian fits to the data.

In the context of other high-field experiments, note that quantum oscillations (QOs) have been observed (23, 28) in ortho-II crystals (with $T_c \sim 58$ to 60 K) in fields above 18 to 22 T, $\sim H_{3D}$. Thus, it seems that H_{3D} is always less than or equal to the lowest fields at which QOs occur, and the QOs coexist with 3D CDW order, although it is presently unclear whether the QOs arise in the portions with 2D or 3D CDW. Moreover, H_{3D} agrees with

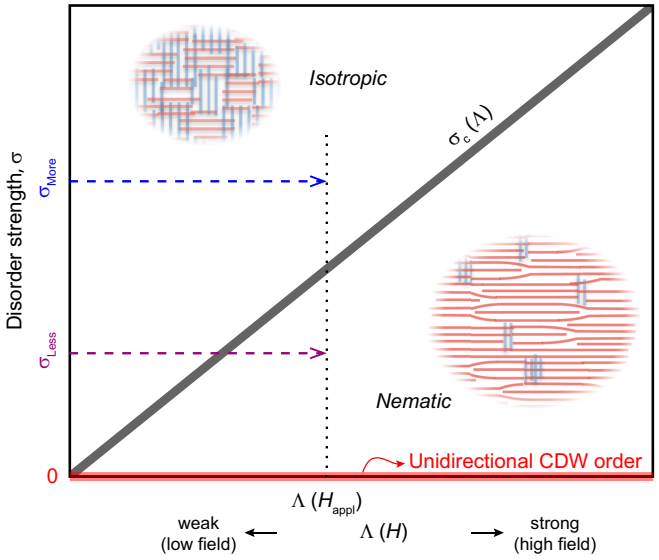

Fig. 5. Schematic CDW phase diagram. Low-temperature phase diagram of a layered crystal as a function of disorder strength (σ) and CDW strength, $\Lambda(H)$, assumed to be an increasing function of increasing *H*, due to the suppression of the superconductivity. It is assumed that the disorder-free state (marked by the red-colored bar on the *x* axis) is an incommensurate, unidirectional CDW. In a tetragonal crystal, the thick gray line marks a nematic transition, σ_c, whereas in a weakly orthorhombic YBCO crystal it is a cross-over. Above σ_c, CDW correlations are short-ranged and bidirectional. Insets show the cartoons of disorder-pinned CDW domains; approximately isotropic, bidirectional, CDW phase (top left) and sharply defined nematic, unidirectional phase (bottom right). In the context of the proposed inhomogeneity scenario, the purple and blue dashed arrows demonstrate the field-dependent CDW evolution in the less (σ_{Less}) and more (σ_{More}) disordered regions of the sample. At a given applied magnetic field (H_{appl}), the σ_{Less} region transforms from the bidirectional 2D CDW into the unidirectional 3D CDW order, whereas the σ_{More} region remains in the isotropic phase (see also *SI Appendix* and *SI Appendix*, Fig. S1).

the Fermi surface reconstruction field deduced from Hall coefficient measurements (29). Although the proposed inhomogeneity picture qualitatively captures our experimental observations, it is not obvious that the Cu and O lines in NMR are readily interpreted as the sum of contributions from a unidirectional and a bidirectional CDW (4, 6, 21). We tentatively suggest that this reflects the fact that the local CDW correlations—to which NMR is most sensitive—are similar in the more- and less-disordered regions, and that it is only subtle, long-distance correlations that distinguish them.

This worry aside, our results strongly suggest that the ground state competing order in "ideal" superconducting YBCO with zero disorder would be a long-range ordered, incommensurate, unidirectional CDW. Our results also lend support to the existence of nematic components in the proximate phases to the 3D CDW in the phase diagram, and to their interpretation as arising from remnant unidirectional 3D CDW correlations (19, 30).

Materials and Methods

Samples. Detwinned single crystals of $YBa_2Cu_3O_{6.51}$ (ortho-II, $T_c = 57$ K, doping concentration $p \sim 0.1$) and $YBa_2Cu_3O_{6.67}$ (ortho-VIII, $T_c = 67$ K, $p \sim 0.12$) were studied. We note that YBCO crystals generally belong to the cleanest available cuprate among the different families (31). The single crystals were obtained from flux growth (32). For two reflection geometries (shown in *SI Appendix*, Fig. S4), two crystals were prepared for each doping. The longest dimensions of crystals were parallel to the crystallographic *a* axis and *b* axis in $(0, k, l)$ and $(h, 0, l)$ reflection geometry, respectively, while applying the magnetic field H along the *c* axis. Note that we prepared thin crystals (less than 0.5 mm) along the *b*- and *a*-axis to avoid sample heating via eddy currents due the pulsed magnetic field.

Resonant Soft X-Ray Scattering Under Zero Magnetic Field. The quasi-2D CDW from these crystals were characterized by resonant soft X-ray scattering (RSXS) measurements at the Cu L_3-edge (931 eV; maximum energy position of X-ray absorption spectroscopy) at beamline 13-3 of the Stanford Synchrotron Radiation Lightsource as shown in Fig. 1*A*. Note that the obtained data were from theta (sample) scans at fixed detector angle 176°. An *l*-value of ∼1.45 r.l.u., that is, slightly less than the half-integer value, had to be chosen due to experimental constraints and the limited total momentum transfer at $E = 931$ eV. All RSXS data backgrounds are subtracted by references that were measured at 150 K. Solid lines are Gaussian fits to the data with a linear background.

Pulsed High-Magnetic-Field X-Ray Scattering. The experimental setup is essentially the same as that used in our previous work (13) and the scattering geometry for the X-ray scattering with a pulsed magnetic field is shown in *SI Appendix*, Fig. S4. The high-magnetic-field experiment was performed at the X-ray Correlation Spectroscopy instrument of the Linac Coherent Light Source at the SLAC National Accelerator Laboratory (33). We use the pink beam with an incident photon energy of 8.8 keV and a horizontally (σ) polarized X-ray, just below the Cu *K*-edge to reduce the fluorescence background from copper. The pink beam gives higher photon flux that enables single-shot-pulsed-field experiments. The momentum resolution is limited by both broad energy bandwidth (∼30 eV) of the pink beam and the beam divergence. Note that the energy bandwidth in our previous measurement (13) was ∼50 eV. Femtosecond X-ray pulses were synchronized to arrive at the sample when the magnetic field pulse reached the maximum. Note that the maximum strength of magnetic field in this work is 32.1 T, which is higher than our previous work (13).

Data Acquisition. All field-applied data were collected by synchronizing a magnetic pulse and X-ray pulse (13). To obtain the zero-field background, diffraction patterns were collected before and after the magnetic pulse. In the main text, all difference maps of diffraction patterns are produced by subtracting the zero-field data. As an example, field-applied and zero-field diffraction intensity maps of Fig. 1*C* are shown in *SI Appendix*, Fig. S2.

ACKNOWLEDGMENTS. This work was supported by Department of Energy (DOE), Office of Science, Basic Energy Sciences, Materials Sciences and Engineering Division Contract DE-AC02-76SF00515. X-ray FEL studies were carried out at the Linac Coherent Light Source, a Directorate of SLAC and an Office of Science User Facility operated for the US DOE, Office of Science by Stanford University. Resonant soft X-ray scattering measurements were carried out at the Stanford Synchrotron Radiation Lightsource (BL13-3), a Directorate of SLAC and an Office of Science User Facility operated for the US DOE, Office of Science by Stanford University. This work was also supported by KAKENHI Grants 23224009, 15K13510, ICC-IMR, and MD program (to H.N.); and US DOE, Office of Basic Energy Sciences, Division of Materials Sciences and Engineering, Award DE-FG02-99ER45772 (to C.A.B.). Materials development was supported by the Natural Sciences and Engineering Research Council and by the Canadian Institute for Advanced Research.

1. Tranquada JM, Sternlieb BJ, Axe JD, Nakamura Y, Uchida S (1995) Evidence for stripe correlations of spins and holes in copper oxide superconductors. *Nature* 375(6532):561–563.
2. Hoffman JE, et al. (2002) A four unit cell periodic pattern of quasi-particle states surrounding vortex cores in $Bi_2Sr_2CaCu_2O_{8+\delta}$. *Science* 295(5554):466–469.
3. LeBoeuf D, et al. (2007) Electron pockets in the Fermi surface of hole-doped high-T_c superconductors. *Nature* 450(7169):533–536.
4. Wu T, et al. (2011) Magnetic-field-induced charge-stripe order in the high-temperature superconductor $YBa_2Cu_3O_y$. *Nature* 477(7363):191–194.
5. LeBoeuf D, et al. (2013) Thermodynamic phase diagram of static charge order in underdoped $YBa_2Cu_3O_y$. *Nat Phys* 9(2):79–83.
6. Wu T, et al. (2013) Emergence of charge order from the vortex state of a high-temperature superconductor. *Nat Commun* 4:2113.
7. Ghiringhelli G, et al. (2012) Long-range incommensurate charge fluctuations in $(Y,Nd)Ba_2Cu_3O_{6+x}$. *Science* 337(6096):821–825.
8. Chang J, et al. (2012) Direct observation of competition between superconductivity and charge density wave order in $YBa_2Cu_3O_{6.67}$. *Nat Phys* 8(12):871–876.
9. Comin R, et al. (2014) Charge order driven by Fermi-arc instability in $Bi_2Sr_{2-x}La_xCuO_{6+\delta}$. *Science* 343(6169):390–392.
10. Neto EHdS, et al. (2014) Ubiquitous interplay between charge ordering and high-temperature superconductivity in cuprates. *Science* 343(6169):393–396.
11. Tabis W, et al. (2014) Charge order and its connection with Fermi-liquid charge transport in a pristine high-Tc cuprate. *Nat Commun* 5:5875.
12. Croft TP, Lester C, Senn MS, Bombardi A, Hayden SM (2014) Charge density wave fluctuations in $La_{2-x}Sr_xCuO_4$ and their competition with super conductivity. *Phys Rev B* 89(22):224513.
13. Gerber S, et al. (2015) Three-dimensional charge density wave order in $YBa_2Cu_3O_{6.67}$ at high magnetic fields. *Science* 350(6263):949–952.
14. Chang J, et al. (2016) Magnetic field controlled charge density wave coupling in underdoped $YBa_2Cu_3O_{6+x}$. *Nat Commun* 7:11494.
15. Blackburn E, et al. (2013) X-ray diffraction observations of a charge-density-wave order in superconducting ortho-II $YBa_2Cu_3O_{6.54}$ single crystals in zero magnetic field. *Phys Rev Lett* 110(13):137004.
16. Blanco-Canosa S, et al. (2014) Resonant X-ray scattering study of charge-density wave correlations in $YBa_2Cu_2O_{6+x}$. *Phys Rev B* 90(5):054513.
17. Comin R, et al. (2015) Broken translational and rotational symmetry via charge stripe order in underdoped $YBa_2Cu_3O_{6+y}$. *Science* 347(6228):1335–1339.
18. Fradkin E, Kivelson SA, Tranquada JM (2015) Colloquium: Theory of intertwined orders in high temperature superconductors. *Rev Mod Phys* 87(2):457–482.
19. Nie L, Tarjus G, Kivelson SA (2014) Quenched disorder and vestigial nematicity in the pseudogap regime of the cuprates. *Proc Natl Acad Sci USA* 111(22):7980–7985.
20. Maharaj AV, Hosur P, Raghu S (2014) Crisscrossed stripe order from interlayer tunneling in hole-doped cuprates. *Phys Rev B* 90(12):125108.
21. Wu T, et al. (2015) Incipient charge order observed by NMR in the normal state of $YBa_2Cu_3O_y$. *Nat Commun* 6:6438.
22. Grissonnanche G, et al. (2014) Direct measurement of the upper critical field in cuprate superconductors. *Nat Commun* 5:3280.
23. Maharaj AV, Zhang Yi, Ramshaw BJ, Kivelson SA (2016) Quantum oscillations in a bilayer with broken mirror symmetry: A minimal model for $YBa_2Cu_3O_{6+\delta}$. *Phys Rev B* 93(9):094503.
24. Ando Y, Segawa K, Komiya S, Lavrov AN (2002) Electrical resistivity anisotropy from self-organized one dimensionality in high-temperature superconductors. *Phys Rev Lett* 88(13):137005.
25. Daou R, et al. (2010) Broken rotational symmetry in the pseudogap phase of a high-Tc superconductor. *Nature* 463(7280):519–522.
26. Hinkov V, et al. (2008) Electronic liquid crystal state in the high-temperature superconductor $YBa_2Cu_3O_{6.45}$. *Science* 319(5863):597–600.
27. Hamidian MH, et al. (2015) Magnetic-field induced interconversion of cooper pairs and density wave states within cuprate composite order. arXiv:1508.00620 [cond-mat].
28. Sebastian SE, et al. (2011) Chemical potential oscillations from nodal Fermi surface pocket in the underdoped high-temperature superconductor $YBa_2Cu_3O_{6+x}$. *Nat Commun* 2:471.
29. Grissonnanche G, et al. (2015) Onset field for Fermi-surface reconstruction in the cuprate superconductor YBCO. arXiv:1508.05486 [cond-mat].

30. Scalapino DJ (2014) Remnant of stripe order. *Proc Natl Acad Sci USA* 111(22): 7886–7887.
31. Vojta M (2009) Lattice symmetry breaking in cuprate superconductors: Stripes, nematics, and superconductivity. *Adv Phys* 58(6):699–820.
32. Liang R, Bonn DA, Hardy WN (2012) Growth of YBCO single crystals by the self-flux technique. *Phil Mag* 92(19–21):2563–2581.
33. Alonso-Mori R, et al. (2015) The X-ray Correlation Spectroscopy instrument at the Linac Coherent Light Source. *J Synchrotron Radiat* 22(3):508–513.